A&A manuscript no.
(will be inserted by hand later)

Your thesaurus codes are:
03(08.03.4, 08.13.2, 08.16.4, 11.13.1, 13.09.6)

ASTRONOMY
AND
ASTROPHYSICS
17.8.1998

Near-infrared photometry and optical spectroscopy of IRAS sources in the Small Magellanic Cloud ⋆

M.A.T. Groenewegen[1] **and J.A.D.L. Blommaert**[2]

[1] Max-Planck-Institut für Astrophysik, Karl-Schwarzschild-Straße 1, D-85740 Garching, Germany
[2] ISO Science Operations Centre, Astrophysics Division of ESA, Villafranca, PO Box 50727, E-28080 Madrid, Spain

received, accepted

Abstract. Near-infrared photometry is obtained of 30 IRAS sources in the direction of the Small Magellanic Cloud selected to be possible AGB stars. Low resolution 4000 to 10 000 Å spectroscopy is presented for 10 of them, plus two AGB stars in the LMC. Improved IRAS fluxes are obtained using the GIPSY package.

Based on the optical spectra and analyses of colour-colour diagrams 9 are confirmed or likely carbon stars, and 8 are confirmed or likely oxygen-rich AGB stars. In three cases no near-infrared counterpart could be identified. The remaining 10 objects have the colours of mass-losing AGB stars, but not enough information is available to comment on the chemical type. In two of these cases there is a mismatch between the near-infrared and IRAS colours possibly indicating unusually large variability, or misidentification of the IRAS sources.

Key words: circumstellar matter – stars: mass loss – stars: AGB – Magellanic Cloud – Infrared: stars

1. Introduction

Searches for Asymptotic Giant Branch (AGB) stars in the Magellanic Clouds (MCs) have been made using optical spectroscopic surveys (e.g. Blanco et al. 1980, Blanco & McCarthy 1991, Rebeirot et al. 1993 [RAW], Morgan & Hatzidimitriou 1995), photometric surveys using V and I Schmidt plates (e.g. Reid et al. 1987) and optical surveys for LPVs (e.g. Payne-Gaposhkin 1971; Hughes 1989). However, these surveys missed the red dust-enshrouded OH/IR stars and infrared carbon stars in the MCs, very luminous examples of which did turn up in the IRAS point source catalog. Recently, near-infrared studies have been initiated to study IRAS sources in the MCs (Reid et al. 1990, Reid 1991, Wood et al. 1992 [W92], Zijlstra et al. 1996 [Z96], Loup et al. 1997, Tanabé et al. 1997). Still, most work until now focussed on the Large Magellanic Cloud. The existing data on IRAS selected AGB star candidates in the SMC can be found in Whitelock et al. (1989, WFMC), Wood et al. (1992) and Z96. As the metallicity difference between the SMC and our Galaxy is much larger than that between the LMC and our Galaxy, the SMC AGB stars are interesting in the study of the influence of metallicity on AGB evolution. As an example of this, Groenewegen et al. (1995) compared the spectral energy distribution and 8-13 μm spectra of an AGB star of comparable pulsation period in the galaxy, LMC and SMC and showed that the dust optical depth of the LMC star was two-thirds of that of the Galactic one, but that of the SMC star only one-fifteenth.

In this paper a sample of about 30 red candidate AGB stars in the SMC is selected for which JHK and partly L photometry is obtained. For a subsample optical spectroscopy is presented. In future papers additional ground-based and ISO observations will be presented.

2. Target selection

As AGB stars with significant mass loss radiate predominantly in the mid-infrared the starting point of the selection is the IRAS faint source catalog (FSC; Moshir et al., 1989). All stars in the FSC in the direction of the Small Magellanic Cloud were selected that have a flux-quality of 2 or larger at 12 and 25 μm. As AGB stars that have a 60 μm flux larger than their 25 μm flux are extremely rare in our galaxy, all objects which have $S_{60} > S_{25}$ and a flux-quality of 2 or larger at 60 μm were eliminated as well. This resulted in a sample of 51 stars, which may still contain foreground objects.

To get a rough estimate of the mass loss rate and luminosity of the objects if they were AGB stars in the SMC, the 12 and 25 μm fluxes were fitted to a pre-calculated grid of simple radiative transfer models (Groenewegen 1993). A central star represented by a black body of 2500 K was assumed to be surrounded by a circumstellar shell containing carbon dust. For the level of modelling used it is of little importance that some

Send offprint requests to: M. Groenewegen, groen@mpa-garching.mpg.de

⋆ Based on observations obtained at the European Southern Observatory at La Silla, Chile under programs 56.E-0325 and 58.E-0274.

of the objects are oxygen-rich and where a model with silicate dust would have been more appropriate. The temperature of the dust at the inner radius was assumed to be 1000 K. In such a model the S_{12}/S_{25} ratio is completely determined by the dust optical depth. For a fixed distance the luminosity of the object is immediately derived by comparing the calculated with the observed 12 μm flux.

For every star the luminosity and optical depth (mass loss rate) were estimated in this way. Candidate AGB stars are those that have luminosities below, say, 10^5 L$_\odot$ (to allow for the fact that the luminosity estimate may be wrong by up to a factor of two and that some IRAS sources are Mira variables whose IRAS fluxes may represent the flux close to maximum light) and mass loss rates in the range 10^{-7}-10^{-4} M$_\odot$ yr^{-1}. In this scheme foreground objects typically have low mass loss rates and very high fiducial luminosities. Every result was inspected individually to check if no potential AGB stars were inadvertently left out. In addition every star was run through the SIMBAD database to look for any additional information. Two stars are included in the sample that are known foreground objects; both are late-type giants and NIR photometry may be of interest. Apart from presenting the photometry these stars are not discussed further. In addition four stars with a flux-quality of only one at 12 or 25 μm were included.

The final sample of candidate AGB stars in the SMC contains 31 objects. This sample is not intended or expected to be complete and may still contain a few foreground objects (apart from the two known ones). Table 1 lists our designation, the name in the FSC, and the IRAS 12 and 25 μm fluxes derived using the GIPSY package as explained in Sect. 5.

Table 1. The sample

Id.[(1)]	FSC name	S_{12}[(2)] (Jy)	S_{25}[(2)] (Jy)
S1	00271–7120	0.27 ± 0.01	0.095 ± 0.003
S2	00350–7436	0.33 ± 0.02	0.30 ± 0.02
S3	00356–7308	0.15 ± 0.01	0.085 ± 0.009
S4	00393–7326	0.17 ± 0.02	0.065 ± 0.014
S5	00448–7344	0.13 ± 0.01	0.108 ± 0.008
S6	00448–7332	0.18 ± 0.01	0.16 ± 0.01[(3)]
S7	00454–7257	0.22 ± 0.01	0.14 ± 0.01
S8	00468–7427	0.10 ± 0.01	0.072 ± 0.009
S9	00483–7347	0.62 ± 0.03	0.46 ± 0.01
S10	00486–7308	0.41 ± 0.02	<0.6[(3)]
S11	00490–7405	0.17 ± 0.01	0.096 ± 0.006
S12	00491–7246	0.051 ± 0.008	0.23 ± 0.01
S13	00492–7408	0.11 ± 0.01	0.18 ± 0.01
S14	00530–7421	0.089 ± 0.010	0.087 ± 0.006
S15	00535–7219	0.20 ± 0.01	0.14 ± 0.01
S16	00554–7351	0.36 ± 0.01	0.21 ± 0.01
S17	00557–7309	0.16 ± 0.01	0.098 ± 0.004
S18	00591–7307	0.15 ± 0.01	0.102 ± 0.007
S19	01027–7231	0.16 ± 0.01	0.042 ± 0.004
S20a	01066–7332	0.15 ± 0.004	0.083 ± 0.004
S20b			
S21	01067–7308	0.24 ± 0.01	0.17 ± 0.003
S22	01074–7140	0.36 ± 0.02	0.43 ± 0.01
S23	01091–7320	0.11 ± 0.01	0.14 ± 0.01
S24	01160–7451	0.17 ± 0.01	0.11 ± 0.01
S25	00388–7401	0.19 ± 0.01	0.081 ± 0.004
S26	01014–7218	0.17 ± 0.01	0.21 ± 0.01
S27	01015–7222	0.23 ± 0.01	0.58 ± 0.02
S28	01042–7215	0.15 ± 0.01	0.50 ± 0.02
S29	01082–7335	0.19 ± 0.01	0.10 ± 0.01
S30	01210–7125	0.166 ± 0.005	0.062 ± 0.003
S31	01238–7218	0.18 ± 0.01	0.060 ± 0.003

[1]Our own designation; [2]IRAS fluxes determined from the GIPSY package as explained in Sect. 5. [3]IRAS flux contaminated.

3. Observations

3.1. Near-infrared photometry

The observations were performed using the ESO/MPI 2.2m telescope at La Silla, Chile. On October 14 and 15, 1995 the 256×256 pixel HgCdTe NICMOS-3 array IRAC2 was used to obtain the JHK photometry. A pixel size of 0.27″ was chosen resulting in a field of view of 69×69″. Both nights were photometric.

For each object the field was centered on the IRAS coordinates and the on-line display was used to identify the counterpart using the J and K filter (by default the infrared counterpart to the IRAS source is assumed to be the reddest star in the field). If necessary the telescope was moved slightly to place the star somewhat nearer to the center of the field. Five images were taken in JHK each, one at the center position and four dithered by ± 10″ in RA and Dec. The five images were median filtered to give the sky emission which was subsequently subtracted from the five object frames. The resulting frames were divided by the flatfield and bad pixels were removed. Flat fields were obtained by subtracting an image of the screen in the dome from one where the screen was illuminated by a lamp.

The assumed counterpart was identified, and four images were shifted by an integer number of pixels to coincide with the counterpart on the fifth image. The five resulting images were then averaged. Software aperture photometry was used to obtain the flux within the aperture.

The typical integration times are 5×10 seconds on chip exposure time per image for JHK. For the brighter sources this was adjusted accordingly to avoid saturation. For the weaker sources in J, longer exposure times or a second set of 5 dithered images was taken.

We observed one standard star from the list of standards prepared for the ISO mission, i.e. HD 1274 (listed as having J = 8.807; H = 8.460; K = 8.370). We planned to observe HD 7644 as well but as we found out after the observing run the coordinates listed in the file of standard stars were wrong (listed with a declination of –54° instead of –45°). So instead we unknowingly observed a field star. The error was not apparent during the run because the unknown object turns out to have magnitudes similar to HD 7644 and the coordinates listed for HD 7644 were only accurate to 1′. Both stars were observed

Table 2. Near-infrared photometry

Id.	Position (J2000)	J	H	K	$L^{(1)}$	$\Delta^{(2)}$ ($''$)	remark
S1	0h29m20.2s –71d03′48″	<17.9	16.35 ± 0.11	13.64 ± 0.04	NO	10	
S2	0h36m59.6s –74d19′50″	11.41 ± 0.02	10.27 ± 0.02	9.14 ± 0.02	7.3 ± 0.6	15	yes
S3	0h37m33.5s –72d52′40″	<17.0	<16.6	14.63 ± 0.07	NO	33	
S4	0h41m16.2s –73d10′09″	14.73 ± 0.05	12.52 ± 0.03	10.60 ± 0.02	8.11 ± 0.06	16	
S5	0h46m47.7s –73d27′56″	18.73 ± 0.28	17.52 ± 0.18	15.45 ± 0.09	NO	41	yes
S6	0h46m41.6s –73d16′47″	16.79 ± 0.12	14.25 ± 0.04	12.10 ± 0.02	NO	25	
S7	0h47m19.2s –72d40′35″	15.61 ± 0.10	13.95 ± 0.04	11.99 ± 0.03	ND	21	yes
S8	0h48m35.2s –74d10′43″	<17.9	18.9 ± 0.3	13.93 ± 0.05	NO	3	
S9	0h50m08.7s –73d31′29″	12.11 ± 0.02	10.42 ± 0.02	9.10 ± 0.02	7.04 ± 0.06	13	yes
S10	0h50m30.7s –72d51′30″	10.66 ± 0.01	9.77 ± 0.02	9.08 ± 0.02	NO	27	yes
S11	0h50m49.1s –73d48′56″	<18.6	17.58 ± 0.18	15.04 ± 0.08	NO	18	
S12	0h50m57.5s –72d30′12″	13.00 ± 0.02	11.97 ± 0.02	11.25 ± 0.02	ND	16	yes
S13	0h50m57.3s –73d51′53″$^{(3)}$						yes
S14	0h54m43.3s –74d04′54″	15.35 ± 0.07	14.06 ± 0.04	12.86 ± 0.03	ND	19	
S15	0h55m17.7s –72d03′11″	14.41 ± 0.04	13.92 ± 0.04	12.68 ± 0.03	NO	12	yes
S16	0h57m04.6s –73d35′12″	14.71 ± 0.05	12.34 ± 0.03	10.30 ± 0.02	7.75 ± 0.07	5	yes
S17	0h57m28.1s –72d53′30″	15.64 ± 0.08	13.35 ± 0.03	11.29 ± 0.02	9.3 ± 0.3	3	
S18	1h00m48.1s –72d51′02″	9.63 ± 0.01	8.71 ± 0.02	8.30 ± 0.02	8.4 ± 0.2	5	yes
S19	1h04m21.2s –72d15′10″	6.48 ± 0.01	6.83 ± 0.02	6.34 ± 0.02	NO	7	yes
S20a	1h08m10.3s –73d15′52″	11.08 ± 0.01	10.00 ± 0.02	9.39 ± 0.02	8.6 ± 0.2	18	
S20b	1h08m08.8s –73d16′18″	12.95 ± 0.02	12.00 ± 0.02	11.56 ± 0.02	ND	9	yes
S21	1h08m17.8s –72d52′56″$^{(3)}$						yes
S22	1h09m02.3s –71d24′10″	11.50 ± 0.02	10.74 ± 0.02	10.25 ± 0.02	9.7±0.3	22	yes
S23	1h10m32.4s –73d05′05″	<18.4	16.05 ± 0.10	13.42 ± 0.04	NO	31	
S24	1h17m17.3s –74d36′17″	16.74 ± 0.12	14.35 ± 0.05	11.81 ± 0.02	NO	4	
S25	0h40m44.6s –73d45′23″	18.23 ± 0.23	14.85 ± 0.06	12.59 ± 0.03	NO	7	
S26	1h03m07.8s –72d02′20″	16.13 ± 0.09	15.31 ± 0.07	14.79 ± 0.07	NO	3	yes
S27	1h03m07.4s –72d06′30″	15.70 ± 0.09	15.18 ± 0.07	13.30 ± 0.04	ND	12	yes
S28	1h05m50.1s –71d59′50″	16.66 ± 0.12	15.74 ± 0.08	13.18 ± 0.03	NO	26	yes
S29	1h09m40.3s –73d19′27″$^{(3)}$						yes
S30	1h22m29.3s –71d09′38″	15.41 ± 0.07	13.48 ± 0.03	11.42 ± 0.03	ND	9	
S31	1h25m10.2s –72d03′13″	7.15 ± 0.01	NO	6.46 ± 0.02	NO	3	yes

[1] NO = not observed; ND = not detected; [2] Distance between IRAS position and the IR position in column 2; [3] IRAS FSC coordinates.

Remarks:
S2: SMC 5, see WFMC (likely carbon-rich) and Z96; S5: Red object but probably not IRAS counterpart; S7: SMC 40 ?; S9: SMC 61, see WFMC; S10: SMC 65, GM 103, see G95; S12: SMC 71, RAW 644 (C); S13: No red star in field; S15: N 55, symbiotic star; S16: SMC 119, see WFMC (800 day LPV); S18: SMC 139 ?, HV 11417 (M5e); S19: G8/K0 III foreground star; S20b: RAW 1543 (C); S21: close to cluster NGC 419; S22: SMC 185, HV 12956, see WFMC, Z96; S26: S26 & S27 appear to lie on a large extended IRAS structure; S27: see S26. NIR photometry possibly contaminated by nearby sources; S28: SMC 176; S29: No red star in field; S31: K1/K2 III foreground star.

at several air masses to obtain the extinction coefficients. Inspection of the count rates of both stars at roughly the same air masses on both nights showed no significant variations. It was decided to combine the standard star observations of both nights to determine the extinction coefficients and zero points. The extinction coefficients determined for both stars were comparable.

They were subsequently averaged and the zero points derived from HD 1274 are used. The unknown object (located approximately at RA = 1h15m36s, δ = –54°26.0′, J2000) has magnitudes J = 9.80, H = 9.40, K = 9.27.

The resulting photometry is listed in Table 2. The error quoted is the error due to the uncertainties in the determination of the zero point and extinction coefficient (0.01 in J and 0.02 in H and K) and Poisson noise. In case of upper limits the weakest detected object in the field is taken as a measure of the upper limit. The designation of the sources is ours.

On October 16 and 17, 1995 L images were obtained for a selected number of sources using the 58×62 pixel InSb SRBC IRAC1 array on the 2.2m telescope. A pixel size of 0.45″ was chosen resulting in a field of view of 26×28″. Initially we intended to get M images as well but as we were barely able to detect a M = 3.3 standard star, no further M images were taken.

Standard chopping and nodding techniques were used: 15″ E-W at a rate of 12 Hz. This has the advantage that an object

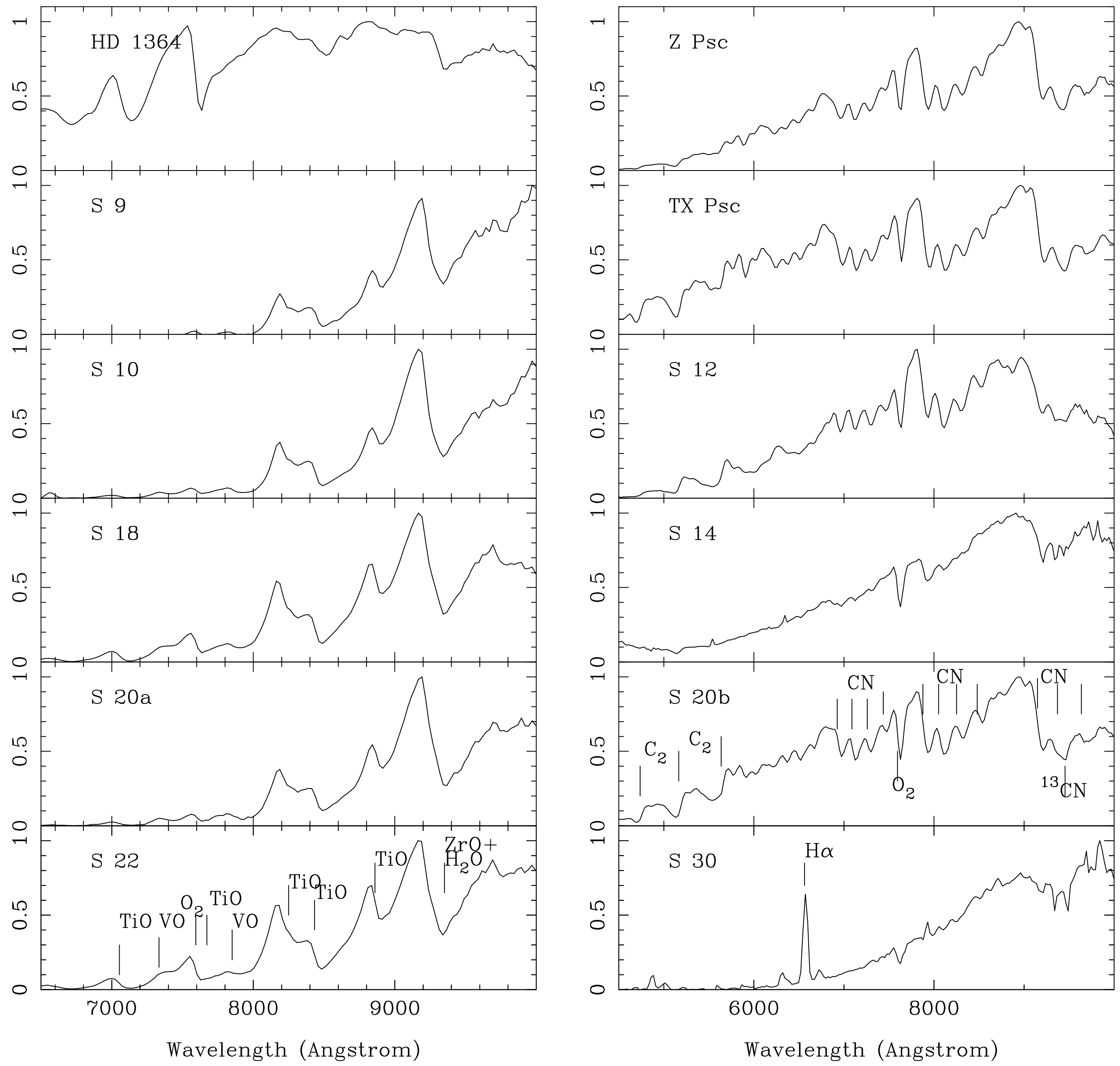

Fig. 1. The optical spectra of the spectral standards and some SMC objects. To the left the oxygen-rich objects, to the right the carbon-rich objects. Some prominent lines are indicated, including telluric O_2 and H_2O.

appears twice in the raw data image: once with positive and once with negative signal. These can then be combined to increase the S/N. The standard star HR 77 (L = 2.792) was observed at several air masses during the two nights.

The observations of the targets and the standard star were constructed in such a way that an object would always appear roughly at the same location of the array. So, instead of constructing a formal flatfield based on the pixel-to-pixel variations a flatfield was determined on a 'region-to-region' basis. This flat field was determined by comparing the count rates of the standard star in these regions. Measurements made at six positions across the array varied by up to 20%. When applying the region-to-region flatfield this was reduced to about 3.5% (1σ). Because of the relative large scatter in the count rates no useful extinction correction could be derived. The fit was consistent with zero extinction and no extinction correction was applied. The derived L magnitudes are listed in Table 2; some of the error bars are large.

3.2. Optical spectroscopy

On October 16 and 17, 1996, optical spectroscopy was obtained for a sub-sample of sources using the EFOSC1 instrument on the 3.6m telescope. The objects observed are those that had a clear optical counterpart. In addition, two AGB stars in the LMC were observed at the end of the nights when the SMC was at a high airmass. They are TRM 88 (Reid et al. 1990) and LI-LMC 57 (Schwering & Israel 1989b)

Acquisition images in the Gunn z band were obtained and compared to the finding charts. The object was identified and placed in a 1.5″ slit. Grism 'B1000' was used. This results in an useful spectral coverage from 3200 to about 10 000 Å with a dispersion of 25 Å per pixel. Flat fields were obtained by illuminating a screen in the dome. Wavelength calibration was achieved using a He/Ar lamp. As the aim was to obtain spectral types no flux standards were observed. The spectral transmission of the atmosphere plus telescope and detector system was obtained by observing EG 21 and LTT 7379. For comparison the well-known carbon stars Z Psc (spectral type C-N5 C_2 4, Barnbaum et al. 1996), TX Psc (C-N5 C_2 4+, Barnbaum et al.) and the M3.5 IIIa MK standard HD 1364 (Keenan & McNeil 1989) were observed. Integration times on the targets were between 10 and 45 minutes. The reduction was carried out with MIDAS.

Most of the SMC star and the comparison spectra are shown in Fig. 1. Figure 2 shows the two LMC stars and the peculiar object S2. S2, S14 and S30 are discussed below. The other cases are straightforward: S9, 10, 18, 20a and 22 are late-type M-giants; S12, 20b and the two LMC AGB stars are carbon stars.

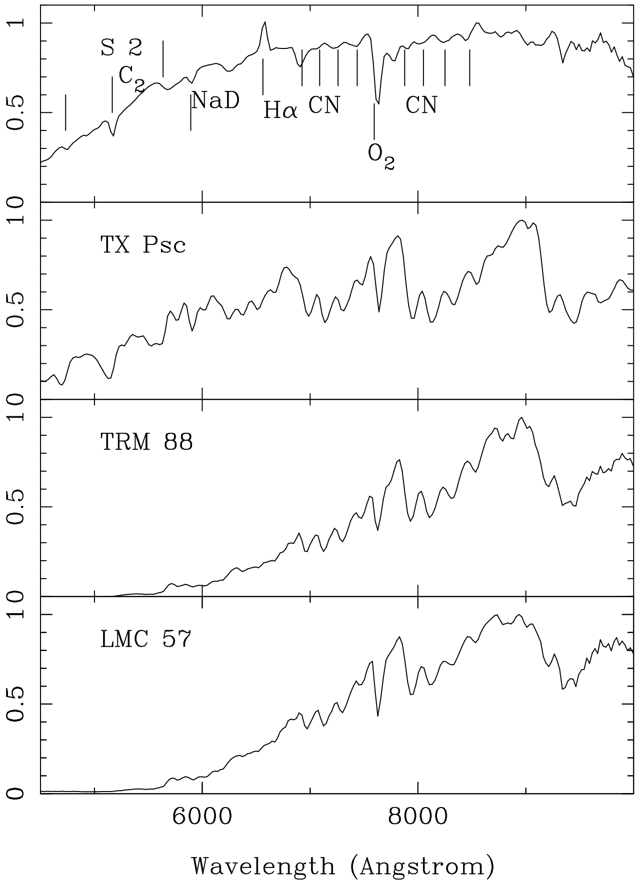

Fig. 2. As Fig. 1 for the peculiar object S2, and the LMC stars.

4. Optical counterparts

The JHK images were compared to optical images constructed from the Digitized Sky Survey (DSS) as offered by ESO through its WWW-page. Although most of the targets do not have a counterpart visible on the DSS image it is possible to derive the coordinates of the targets with an accuracy of about 2″ in RA and Dec with the help of other stars that appear both on the JHK and DSS images. For stars with a visible counterpart on the DSS image the accuracy in the derived coordinates is 1″ or better. The coordinates derived in this way are listed in Table 2. In the case of no identifiable IR counterpart the IRAS coordinates are listed.

The differences between the IRAS-FSC and the NIR coordinates are also listed in Table 2. They are between 3 and 41″. There remains always the possibility that the object of which we list the photometry is not the counterpart of the IRAS source but another red object (foreground or in the SMC).

5. IRAS fluxes

In order to obtain the best possible IRAS 12 and 25 μm fluxes we inspected two-dimensional images and one-dimensional coadds of IRAS scans using the GIPSY software package (Assendorp et al. 1995). The results are listed in Table 1. The error is the 1σ error estimate based on the fluctuation in the background flux. The fluxes from the FSC and as determined using GIPSY are compared in Fig. 3. For the brighter objects the results are essentially identical. At the fainter flux levels the scatter is somewhat larger. The most important change is in the S_{12}/S_{25} ratio. For most stars the colours as derived from GIPSY are bluer than indicated by the FSC fluxes, by on average 8%.

6. Individual objects

The list of stars was correlated with the catalog of Schwering & Israel (1989a). Most stars are not listed there. For those that are, the number is listed in the remarks column as SMC <number>. In most cases their photometry is within 20% of the fluxes derived by us using GIPSY.

The list of objects was compared to the lists of optically selected carbon stars in the SMC of Rebeirot et al. (1993) and Morgan & Hatzidimitriou (1995). Two objects are mentioned in the former publication and none in the latter one. They are RAW 644 (S12) and RAW 1543 (S20b). In the latter case there is another red object in the field (S20a). Although the IRAS source is located closer to S20b, plotting both SEDs suggests that the IRAS colours are related to S20a. This is confirmed by

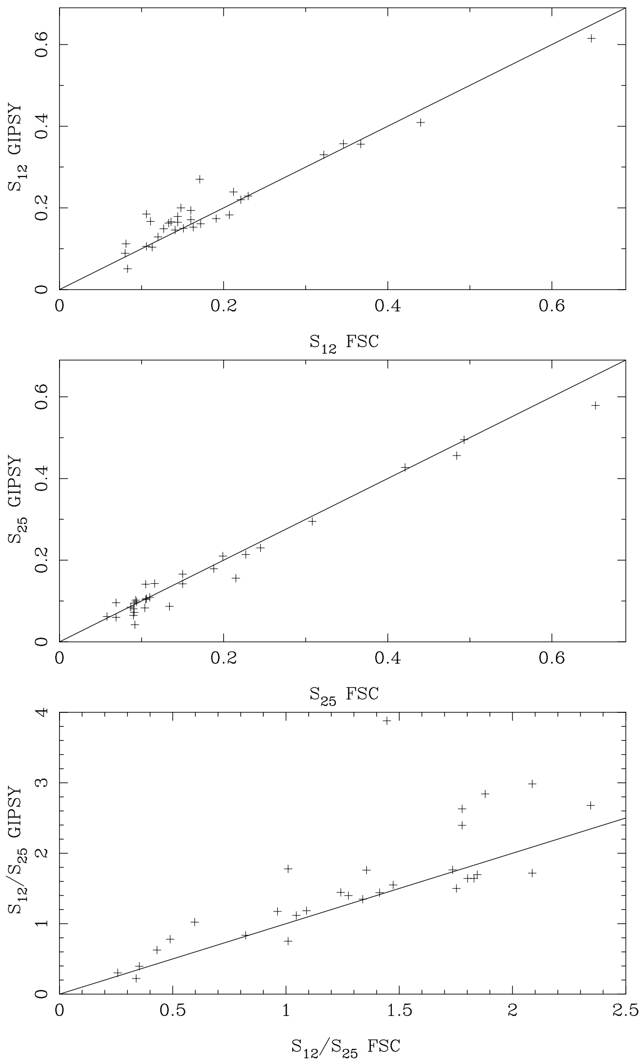

Fig. 3. Comparison between 12, 25 and ratio of 12 to 25 μm flux-densities from the FSC and as determined using the GIPSY package. The lines indicate the one-to-one relations.

our results from ISOCAM imaging where we find a source at 12 micron of comparable flux to the IRAS value at the position of S20a. At the position of S20b only a weak source of order of a few mJy is found in the ISOCAM image.

The counterpart indicated on the finding chart for RAW 644 in Rebeirot et al. is identical to the counterpart identified by us on the NIR images based on the red colours. RAW 644 belongs to the reddest about 20% of stars in their sample. According to the transformation given in RAW the star has a colour of $V - I \approx 2.3$.

The counterpart indicated on the finding chart for RAW 1543 is identical with the counterpart S20b identified by us based on the red colours. RAW 1543 has colours which are average for the carbon stars in RAW's sample. According to the transformation given in RAW the star has a colour of $V - I \approx 1.9$. For both S12 and S20b we confirm the carbon star character from the optical spectra.

The object S2 is interpreted as being carbon-rich according to WFMC. Our photometry is in good agreement with that found by WFMC who also monitored the object and found only minor variations in K. Our data also agrees with the observations in Z96 and van Loon et al. (1997). WFMC present a medium resolution 4000 to 7000 Å spectrum which can be compared to our low resolution spectrum. The major difference with respect to their spectrum is the absence of Hβ. Hα is also much weaker in our spectrum then in theirs (3$\times$ continuum), but this is at least partly due to the lower resolution of our spectrum. Contrary to them we find (weak) CN lines in the spectrum. The overall shape of the SED suggests a temperature similar to that of a late K-giant. The spectral type should be close to C3,2. The new data does not provide any further insight into the evolutionary status of the star.

The object S9 was also monitored by WFMC. It is variable on a long time scale but no period could be derived by them. They derive a high luminosity for this object ($M_{\rm bol} \approx -7.2$) indicating it is a massive AGB star or a supergiant. Our photometry is somewhat fainter than the faintest dataset in their paper. The K-amplitude is of order 0.6 magnitude (WFMC). Our spectrum confirms it to be a late-type M-star.

The object S16 was also monitored by WFMC who found it to be a luminous long-period variable with a K-amplitude of about 1.1 magnitude and a period of about 800 days. Our photometry is in good agreement with that in WFMC.

Our sample also includes the known oxygen-rich stars HV 11417 (S18, spectral type M5e, P = 1300 days, see Elias et al. 1980, 1985), HV 12956 (S22, enhanced in lithium, P = 518 days; see Smith et al. 1995, WBF, WFMC, Z96, van Loon et al. 1997) and GM 103 (S10), in which Groenewegen et al. (1995) detected the silicate feature in emission.

The spectrum of S14 is peculiar (see Fig. 1). It is unmistakably a carbon star because of the presence of the 5165 Å C_2 Swan band and CN band, but these features are very weak. More unusual is the upturn in flux at shorter wavelengths and the emission lines at approximately 5540 Å and 6345 Å This suggests that there may be a binary companion. At the present resolution both lines can not be assigned.

S15 is the VV Cephei type star N55 (Walker 1983). The coordinates of N55 are poorly known but the finding chart in Henize (1956) leaves little doubt that N55 and S19 are identical.

The spectrum of S30 is unusual (see Fig. 1). It shows strong Hα and is very red suggesting a late-spectral type. The blue region is not well exposed and the C_2 bands are not seen. The spectrum is classified as carbon-rich because of the CN bands longward of 9000 Å.

For three objects (S13, S21 and S29) there appears to be no red star in the field. The IRAS coordinates of S21 put this objects close to the edge of the cluster NGC 419, which was clearly visible in our NIR images. It is possible that the IRAS emission is not associated with a single point source. For S13 we have obtained ISOCAM images at different wavelengths indicating an extremely red source close to the IRAS position. Preliminary modelling indicates that it is fainter than 20th magnitude in

K, consistent with the non-detection in the ground-based K-images.

According to information in SIMBAD, the radial velocities of S19 and S31 are such that they are foreground objects of spectral type G8/K0 III (radial velocity of +10 km s^{-1}) and K1/K2 III (radial velocity of –28 km s^{-1}), respectively.

7. Colour-colour-diagrams

In Fig. 4 several often-used colour-colour-diagrams are plotted. In principle they can be used to distinguish between oxygen-rich and carbon-rich objects. The lines in the $(J-H, H-K)$ and $(K-12, H-K)$ colour diagram indicate sequences for Galactic AGB stars that are based on our own work in the case of $(J-H, H-K)$ and taken from van Loon et al. (1997) for $(K-12, H-K)$. There is at least a scatter of 1 magnitude around each of these relations, basically limiting the use of these two colour-colour diagrams as O-/C-separators.

The region where O-rich (indicated by O) and C-rich stars (indicated by C) exist in the $([12]-[25], K-L)$ colour-colour diagram is taken from Epchtein et al. (1987; [12] and [25] in magnitudes). The region occupied by C-stars in the $([12]-[25], J-K)$ diagram was determined by us from Galactic AGB stars. In all these four diagrams the loci and regions are valid for AGB stars with uninterrupted mass-loss. Post-AGB stars, or AGB stars with detached dust shells, can occupy different positions in these diagrams than indicated by their chemistry.

There are some obvious outliers, in particular the known carbon-rich objects S2, S12 and S14 in the $([12]-[25], K-L)$ and $([12]-[25], J-K)$ diagrams. S2 was suggested by WFMC to be a possible post-AGB star and the colours are at least consistent with that: the far-infrared dust shell is still red, but the near-infrared colours are relatively blue. For S14 something similar may be the case. Since S12 has a normal position in the $(K-[12], H-K)$ diagram, its unusual $[12]-[25]$ colour may be due an overestimated 25 μm flux by a factor of 30. This is, admittedly, an unusually large factor.

Based on the location in the colour-colour diagrams one may hypotesize that S4, 16, 24 and 25 are carbon-rich and S27 and 28 are oxygen-rich.

8. Discussion and conclusions

From the IRAS faint source catalog we selected 29 potential AGB stars in the direction of the SMC. Near-infrared photometry was obtained for that sample and two foreground late-type giants. One additional red object was discovered serendipitously. Optical spectroscopy was obtained for a sub-set of stars including two AGB stars in the LMC. Improved IRAS fluxes were obtained using the GIPSY package.

With this sample, it is possible to make a first comparison with AGB stars in the LMC. It turns out that the reddest stars in the SMC are as red as the stars so far found in the LMC. For example, the reddest two LMC AGB stars in Reid (1991) have $(H-K)$ of 3.00 and 2.85, those in Wood et al. (1992) have $(H-K)$ = 2.30 and 2.81, and those in van Loon et al. (1997) have $(H-K)$ = 4.9 ($\pm$1) and 2.9. The reddest objects in our sample have $(H-K)$ = 5.0 and 2.8. This is somewhat surprising as one might have expected that stars in the SMC lose mass at a lower rate because of the lower metallicity. It may be a consequence of the fact that only the most heavily mass-losing stars in the more distant SMC will have been detected by IRAS.

On the other hand, the stars are not as red as the reddest Galactic AGB stars, which reach colours up to $(H-K)$ = 6.0, or $(J-K)$ = 10 (e.g. Fig. 5 in Groenewegen et al. 1997).

Of the 30 AGB star candidates, 5 are known or confirmed as carbon stars (S2,12,14,20b,30) and 6 as oxygen-rich stars (S9,10,15,18,20a,22). Three of these (S2,14,30) carbon stars are peculiar in the sense that the C_2 and CN bands are unusually weak. One of these (S2) had previously been suggested to be in an interacting binary system, or a post-AGB star. This could also be the case for the other two objects. Based on colour-colour diagrams an additional 4 carbon- and 2 oxygen-rich stars are suggested. In three cases no red object could be found near the IRAS position. In one case we have obtained multiwavelength ISOCAM images that show an extremely red object, that indeed could not have been found in K. There always remains the possibility that some of the non-confirmed C-/O-objects are red sources unrelated to the IRAS source. This suspicion is confirmed in a few cases by the unusual position of some objects in the colour-colour diagrams (e.g. S8, 26) which indicate that the NIR photometry does not connect very well with the IRAS fluxes. In order to study this sample further, and in particular to establish the nature of these sources, we are in the process of obtaining multiwavelength ISOCAM images and ISOCAM CVF spectra.

Acknowledgements. MG would like to thank Chris Lidman (ESO, Chile) for excellent support during and after the observations. Jacco Th. van Loon (University of Amsterdam) is thanked for his help in reducing the optical spectra, and R.D. Oudmaijer (Imperial College) for constructive comments. This research has made use of the SIMBAD database, operated at CDS, Strasbourg, France.

The IRAS data were obtained using the IRAS data base server of the Space Research Organization of the Netherlands (SRON) and the Dutch Expertise Center for Astronomical Data Processing funded by the Netherlands Organization for Scientific Research (NWO). The IRAS data base server project was also partly funded through the Air Force Office of Scientific Research, grants AFOSR 86-0140 and AFOSR 89-0320.

Based on photographic data obtained using the UK Schmidt Telescope. The UK Schmidt Telescope was operated by the Royal Observatory Edinburgh, with funding from the UK Science and Engineering Research Council, until 1988 June, and thereafter by the Anglo-Australian Observatory. Original plate material is © the Royal Observatory Edinburgh and the Anglo-Australian Observatory. The plates were processed into the present compressed digital form with their permission. The Digitized Sky Survey was produced at the Space Telescope Science Institute under US Government grant NAG W-2166.

References

Assendorp R., Bontekoe T.R., de Jonge A.R.W., et al., 1995, A&AS 110, 395

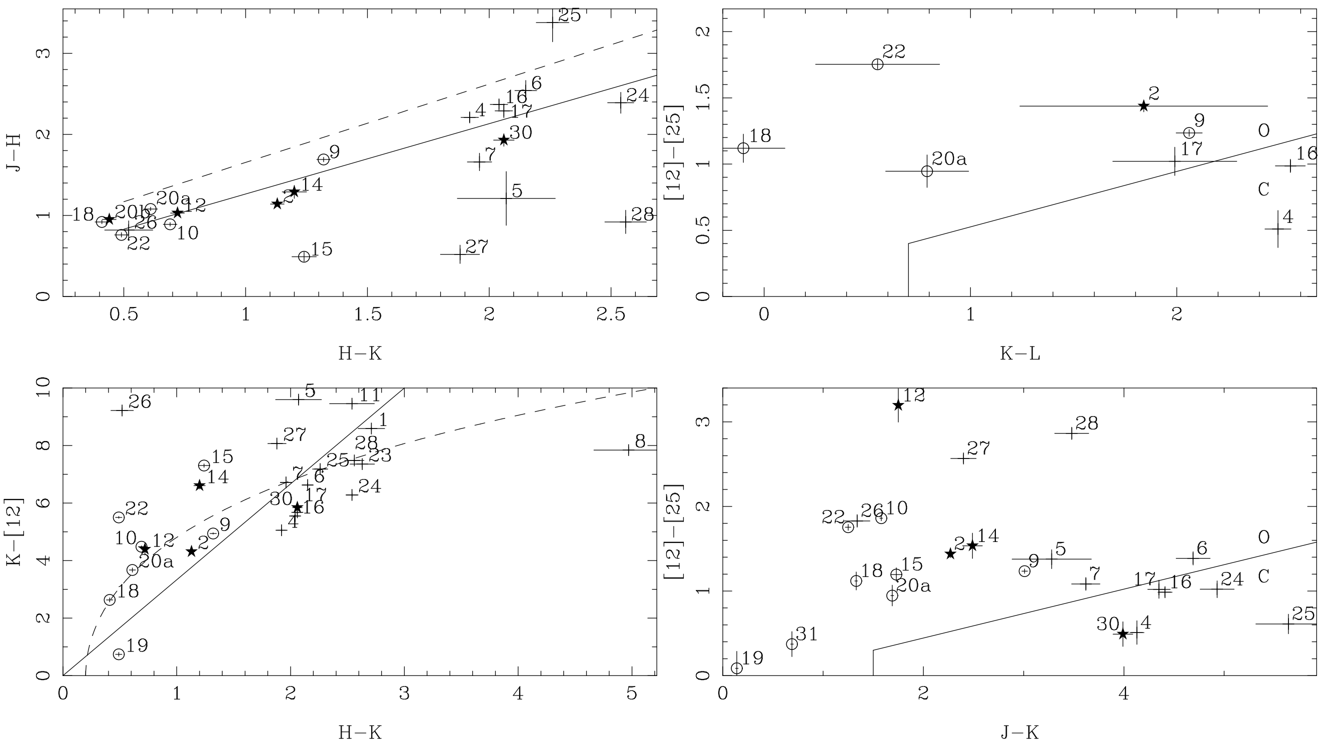

Fig. 4. Colour-colour diagrams. Photometry with errorbars are plotted. Filled stars are known carbon-rich objects; open circles are known oxygen-rich stars. Upper limits on colours are not used. The solid and dashed lines represent the approximate loci of Galactic carbon- and oxygen-rich stars, respectively (see text). Numbers refer to the identification numbers in Table 1.

Barnbaum C., Stone R.P.S., Keenan P.C., 1996, ApJS 105, 419
Blanco V.M., McCarthy M.F., 1991, AJ 100, 674
Blanco V.M., McCarthy M.F., Blanco B.M., 1980, ApJ 242, 938
Elias J.H., Frogel J.A., Humphreys R.A., 1980, ApJ 242, L13
Elias J.H., Frogel J.A., Humphreys R.A., 1985, ApJS 57, 91
Epchtein N., et al., 1987, A&AS 71, 39
Fluks M.A., Plez B., Thé P.S., de Winter D., Steenman H.C., Westerlund B.E., 1994, A&AS 105, 311
Groenewegen, M.A.T., 1993, Ph.D. Thesis, Chapter 5, University of Amsterdam
Groenewegen M.A.T., Smith C.H., Wood P.R., Omont A., Fujiyoshi T., 1995, ApJ 449, L119
Groenewegen M.A.T., Whitelock P.A., Smith C.H., Kerschbaum F., 1997, MNRAS in press
Henize K.G., 1956, ApJS 2, 315
Hughes S.M.G., 1989, AJ 97, 1634
Keenan P.C., McNeil R.C., 1989, ApJS 71, 245
van Loon J.Th., Zijlstra A.A., Whitelock P.A., et al., 1997, A&A 325, 585
Loup C., Zijlstra A.A., Waters L.B.F.M., Groenewegen M.A.T., 1997, A&AS 125, 419
Morgan D.H., Hatzidimitriou D., 1995, A&AS 113, 539
Moshir M., Kopan G., Conrow T., et al., 1989, Explanatory supplement to the IRAS Faint Source Survey, Pasadena: JPL
Pahne-Gaposhkin C.H., 1971, Smithsonian Contr. Ap. 13, 1
Rebeirot E., Azzopardi M., Westerlund B.E., 1993, A&AS 97, 603 (RAW)
Reid N., 1991, ApJ 382, 143
Reid N., Mould J., Thompson I., 1987, ApJ 323, 433
Reid N. Tinney C., Mould J., 1990, ApJ 348, 98
Schwering P.B.W., Israel F.P., 1989a, A&AS 79, 79
Schwering P.B.W., Israel F.P., 1989b, A&AS 79, 105
Smith V.V., Plez B., Lambert D.L., Lubowich D.A., 1995, ApJ 441, 735
Tanabé T., Nishida S., Matsumoto S., et al., 1997, Nature 385, 509
Whitelock P.A., Feast M.W., Menzies J.W., Catchpole R.M., 1989, MNRAS 238, 769 (WFMC)
Walker A.R., 1983, MNRAS 203, 25
Wood P.R., Whiteoak J.B., Hughes S.M.G., Bessell M.S., Gardener F.F., Hyland A.R., 1992, ApJ 397, 552 (W92)
Zijlstra A.A., Loup C., Waters L.B.F.M., Whitelock P.A., van Loon J.Th., Guglielmo F., 1996, MNRAS 279, 32 (Z96)

This article was processed by the author using Springer-Verlag LaTeX A&A style file *L-AA* version 3.